PCCP

Toward elimination of discrepancies between theory and experiment: The gas-phase reaction of N_2O_5 with H_2O

Andreas F. Voegele, Christofer S. Tautermann, Thomas Loerting† and Klaus R. Liedl*

Institute of General, Inorganic and Theoretical Chemistry, University of Innsbruck, Innrain 52a, Austria. E-mail: Klaus.Liedl@uibk.ac.at

Received 13th September 2002, Accepted 6th December 2002
First published as an Advance Article on the web 23rd December 2002

New reaction mechanisms are presented and the corresponding reaction rate constants are calculated for the homogeneous gas-phase reaction $N_2O_5 + nH_2O \leftrightarrow 2HNO_3 + (n-1)H_2O$ with $n = 1,2,3$ using *ab initio* methods and canonical variational transition state theory including tunneling corrections. The reaction barriers for the new mechanisms are 21.1 kcal mol^{-1} for $n = 1$, 18.9 kcal mol^{-1} for $n = 2$ and for the two mechanisms with three water molecules 14.2 and 19.2 kcal mol^{-1}. Using the new reaction mechanism the rate constant for N_2O_5 hydrolysis with $n = 1$ is $k_1 = 5.2 \times 10^{-25}$ cm^3 molecule^{-1} s^{-1} at 298 K, which is in much better agreement with the experimental value being only two orders of magnitude smaller, compared to the old mechanism which is ten orders of magnitude smaller than the experimental value. Also the rate constant for the third order process—second order with respect to [H_2O]—is in better agreement with experiment compared with the old mechanism (seven compared to approximately twelve orders of magnitude). For possible future confirmation of the new reaction mechanisms we determined kinetic isotope effects for the reactions and obtained KIEs of 1.55 and 1.09 for $n = 1$ and $n = 2$ water molecules, respectively, compared to 1.11 and 1.44 for the old mechanisms.

1 Introduction

Nitrogen oxides (NO_x) play an important role in atmospheric chemistry, being involved in several processes. Prominent examples are the formation of nitric acid (HNO_3) in both the stratosphere and troposphere or the involvement in stratospheric ozone depletion.[1–4] One of the key compounds in atmospheric nitrogen oxide chemistry is dinitrogen pentoxide (N_2O_5) which is an important reservoir species for NO_x.[1,5] Formation of N_2O_5 is accomplished by the reaction of nitrogen dioxide with nitrogen trioxide[5]

$$NO_2 + NO_3 \rightleftarrows N_2O_5 \quad (1)$$

The equilibrium of reaction (1) lies on the right side after sun down due to higher NO_2 levels compared to day time, since NO_2 photolysis is shut down and NO is quickly oxidized to NO_2 by O_3.[6–9]

NO_x and stratospheric ozone destruction are coupled together by several mechanisms. For instance, NO_x is part of the "odd nitrogen catalytic cycle" which is responsible for homogeneous ozone depletion.[10–12] However, this effect on total ozone destruction is minute compared to the consequences denitrification has on the active halogen concentration in the stratosphere and thus on ozone destruction: The conversion of actively ozone destroying halogen radicals (mainly ClO_x) into their less active reservoir form ($ClONO_2$) requires an abundance of NO_2 according to the reaction[13,14]

$$ClO + NO_2 \rightleftarrows ClONO_2 \quad (2)$$

Permanent removal of nitrogen oxides from the stratosphere is accomplished by conversion into nitric acid

$$N_2O_5 + H_2O \rightleftarrows 2HNO_3 \quad (3)$$

followed by sedimentation.[1,15] Different kinds of aerosols and polar stratospheric clouds offer a widespread field for heterogeneous conversion reactions of N_2O_5 in the stratosphere: hence several studies have been performed (the results are summarized in Atkinson *et al.*[16] and by the IUPAC Subcommittee for Gas Kinetic Data Evaluation for Atmospheric Chemistry).

Besides heterogeneous reactions there are also several studies on homogeneous reactions of N_2O_5. One of the first investigations on the kinetics of N_2O_5 hydrolysis in the gas phase was carried out by Morris and Niki.[17] They obtained an overall second order rate constant for the reaction of N_2O_5 with H_2O of $k_1 = 1.3 \times 10^{-20}$ cm^3 molecule^{-1} s^{-1} (at 298 K), which is about one order of magnitude larger than the rate constants obtained later on by Tuazon *et al.*, Atkinson *et al.* and Hjorth *et al.* ($1.3–1.5 \times 10^{-21}$ cm^3 molecule^{-1} s^{-1}, 298 K).[18–20] However, the latter rate constants are still larger than the most recent ones due to the contribution of heterogeneous effects that have an enhancing effect on the apparent overall reaction rate. In detailed kinetic studies in a large reaction chamber Mentel, Wahner and co-workers found a second order rate constant for the reaction of N_2O_5 with H_2O of $k_1 = 2.5 \times 10^{-22}$ cm^3 molecule^{-1} s^{-1}. Additionally, they propose an overall third order reaction rate constant (first order in [N_2O_5] and second order in [H_2O]) of $k_2 = 1.8 \times 10^{-39}$ cm^6 molecule^{-2} s^{-1} (293 K).[21,22]

Aside from experimental investigations there are also a few theoretical studies dealing with the reaction of N_2O_5.[23–25] These studies demonstrated that additional water molecules lower the reaction barrier for hydrolysis. McNamara and Hillier[25] found slightly different structures for the N_2O_5 hydrates with higher numbers (*i. e.* $n = 3$, 4) than Snyder *et al.*[24] However, both groups observed the same overall trend of a lower reaction barrier with increasing n, and thus a catalytic effect of water.

This catalytic effect on the reaction of $N_2O_5 + H_2O$ has only been quantified in terms of reaction barriers but not in terms of

† Department of Earth, Atmosphere and Planetary Sciences, Massachusetts Institute of Technology, 77 Massachusetts Avenue, Cambridge, MA 02139-4307, USA.

reaction rates. A detailed quantitative comparison between the theoretical and the experimental homogeneous gas-phase reaction of N_2O_5 with H_2O is therefore not possible. In this study we provide reaction dynamics calculations on the N_2O_5 hydrolysis in the presence of $n = 1$, $n = 2$, and $n = 3$ water molecules by applying variational transition state theory and *ab initio* methods. We deduce the mechanism of the most likely reaction and evaluate the influence of quantum mechanical tunneling on the course of this conversion. Additionally, we determine the kinetic isotope effect for the different reactions.

2 Computational details

2.1 Stationary points

Stationary points were calculated by hybrid density functional theory [B3LYP/6-31+G(d)].[26] The nature of the stationary points was confirmed by vibrational analysis. Saddle points were optimized with the three-structure quadratic synchronous transit guided approach.[27] Due to the underestimation of reaction barriers by (hybrid) density functional theory (DFT) methods such as B3LYP,[28–30] we employed high level methods to evaluate more accurate reaction barriers. Reaction barriers are crucial for describing reaction rates by transition state theory due to an exponential relationship between reaction barrier and reaction rate. Therefore we used Gaussian-2 theory [G2(MP2)][31,32] and Gaussian-3 theory [G3, G3(MP2)//B3LYP and G3//B3LYP][33,34] for most of the studied systems to get more accurate barriers. Both Gaussian-2 and Gaussian-3 theory employ quadratic configuration interaction with single, double and perturbational triple excitations [QCISD(T)] but with different basis sets. G2(MP2) uses the triple zeta 6-311G(d,p) basis set while G3 uses the moderate double zeta 6-31G(d) basis set. The quality of these calculations is improved significantly by basis set extrapolation methods employing MP2 and MP4, respectively, and empirical corrections (these are explained in detail in the original work by Pople and co-workers[31–33]). With these basis set extrapolation methods one gets very good approximations for high level QCISD(T) calculations with the 6-311+G(3df,2p) basis set [for G2(MP2)] and with the G3large basis set [for G3], which is a modified version of the 6-311+G(3df,2p) basis set that includes more polarization functions for the second row (3d2f), less on the first row (2df) and core polarization functions.[33] G3 and G2(MP2) use MP2(Full)/6-31G(d) geometries and scaled HF/6-31G(d) frequencies for further calculations, whereas G3//B3LYP [or G3B3] and G3(MP2)//B3LYP [or G3(MP2)B3] use B3LYP/6-31G(d) geometries and scaled frequencies for further calculations. In a given test set (G2/97) the average absolute deviation from experiment of G3//B3LYP is 0.99 kcal mol^{-1}, of G3 is 1.02 kcal mol^{-1}, of G3(MP2)//B3LYP is 1.25 kcal mol^{-1} and of G2(MP2) is 1.89 kcal mol^{-1}.[33–35] As a fifth high level method we used coupled cluster theory with single, double, and perturbational triple excitations [CCSD(T)/aug-cc-pVDZ][36] on the geometries we obtained at the MP2/aug-cc-pVDZ[37,38] level of theory [CCSD(T)/aug-cc-pVDZ//MP2/aug-cc-pVDZ]. To test for an appropriate choice of the HF reference wave function the performance of CCSD(T)/aug-cc-pVDZ was tested by the $\mathcal{T}_1$ diagnostic.[39]

Normal mode vibrational analysis revealed low frequency vibrations for a few structures. The harmonic oscillator approximation to determine vibrational frequencies often fails for low frequency modes that represent hindered internal rotation.[40] Thus, frequencies that represent hindered internal rotation were identified[41] and the partition functions were determined according to an approximation developed by Truhlar.[42] Considering the number of systems and their size, we used the recommended "Cω single frequency" scheme of Chuang and Truhlar.[40] In this model the effective moment of inertia I_j is determined by a curvilinear (C) model and the barrier for internal rotation W_j is determined from the equation $W_j = 2I_j(\omega_j/M)^2$ where ω_j is obtained from an electronic structure calculation.

2.2 Reaction path

The reaction path was calculated as the steepest descent path starting from the transition state in mass-scaled coordinates where a scaling mass of 1 u was used. To create this so-called minimum energy path (MEP) the local quadratic approximation algorithm of Page and McIver[43] at a step size of 0.050 a_0 (0.026 Å) together with B3LYP/6-31+G(d) was used. Distances on the potential energy surface from the transition state are denoted as s, where s is positive on the product side and negative on the educt side. Second derivatives of the energy with respect to the coordinates and partition functions were calculated every third point along the potential energy surface. Calculation of the path was carried out along both sides of the transition state until the gradient had almost vanished and stable minimum structures were reached. Since B3LYP in general describes geometries and energy hypersurfaces well, but underestimates barrier heights (as mentioned previously), we interpolated the B3LYP/6-31+G(d) hypersurface to the energy values of the stationary points determined at the G3B3 and G3(MP2)B3 level of theory. Calculating the reaction path and thus reaction rates by variational transition state theory based on two different levels of theory is termed dual-level and the interpolation procedure is called variational transition state theory with interpolated corrections. The shorthand notation for this procedure is G3B3///B3LYP/6-31+G(d) and the interpolation procedure is based on a logarithmic procedure.[44]

2.3 Reaction rates and quantum mechanical tunneling

Reaction rates were obtained using variational transition state theory (VTST)[45] as implemented in Polyrate9.0.[46,47] Theoretical details and equations can be found elsewhere:[45,48–52] here we just outline some details. A variational approach for TST with a canonical ensemble was used to obtain a rate constant k^{CVT} (CVT = canonical variational TST) minimized with respect to barrier crossings. When all bound degrees of freedom are described quantum-mechanically, motion along the reaction coordinate cannot be treated quantum-mechanically. Therefore, quantum mechanical effects (mainly tunneling-effects) along the reaction coordinate are treated in good approximation by semiclassical methods to evaluate transmission probabilities. Inclusion of the quantum mechanical effects on the reaction rate constant is carried out by multiplication of the rate constant k^{CVT} with a ground state transmission coefficient κ. The transmission coefficient is evaluated by different methods (that minimize the action integral), which consider that the system tunnels along shorter paths in the course of the reaction that are more demanding in terms of energy. The methods we consider are the small curvature tunneling (SCT) and the large curvature tunneling (LCT) approaches. SCT is investigated by means of the centrifugal dominant small curvature semi-classical adiabatic ground state tunneling method according to the concept of Marcus and Coltrin.[53–55] The LCT correction assumes that tunneling occurs by using a series of straight line connections between the educt and the product valley in the so-called reaction swath. Polyrate employs the large curvature ground state approximation version 4 (LCG4)[56] for LCT. Depending on the curvature of the reaction path and the temperature either SCT or LCT become predominant; thus, one uses the maximum of these methods to evaluate the tunneling corrections and multiplies

it with k^{CVT}. This approach is termed microcanonical optimized multidimensional tunneling (μOMT).

According to the experimental homogeneous gas-phase reaction findings of first and higher order dependence on water vapor pressure and first order dependence on N_2O_5 pressure, the rate of hydrolysis can be considered to be made up of the sum over all nth order dependences on water vapor pressure

$$-\frac{d[N_2O_5]}{dt} = \sum_{n=1}^{i} k_n \times [N_2O_5][H_2O]^n \quad (4)$$

with $n = 1$ and $n = 2$ being the important mechanisms. The rate constant k_n is composed of the tunneling correction factor ($\kappa^{\mu OMT}$), the equilibrium constant for the pre-association (K^{preass}) and the the unimolecular rate constant (k^{CVTST})

$$k_n = \kappa^{\mu OMT} \times K^{preass} \times k^{CVTST} \quad (5)$$

The pre-association equilibrium constant was determined from ΔG^{preass} values calculated at the G3B3 and G3(MP2)B3 levels and converted to the corresponding units by multiplication with the factor $f = (1.363 \times 10^{-22}\ T)^n$ cm^{3n} atm^n (see also Loerting and Liedl.[57]). Additionally we determined the kinetic isotope effect (KIE) for these reactions. The KIE was calculated as the ratio between the "normal" and the deuterated reaction rate constants, and for this purpose the minimum energy path was calculated again and the unimolecular rate constant was determined by VTST, as described above.

Calculations were performed with the Gaussian98[58] program package and with Polyrate9.0[46] and with Gaussrate9.0,[47] which is an interface between Gaussian98 and Polyrate9.0.

3 Results and discussion

3.1 Evaluation of the methods

We determined the pre-association energies for reaction-complex formation and the reaction barriers of N_2O_5 hydrolysis with $n = 1,2,3$ water molecules at several levels of theory (see Tables 1 and 2). For the pre-association energies almost all methods yielded similar results, with the strongest deviation being for reaction channel 2*b* where G2(MP2) and G3B3 deviate by 1.7 kcal mol^{-1}. The standard state free energy changes for pre-association (see Table 1) deviate slightly more, with the largest difference between G3 and G3(MP2)B3 being for reaction channel 2*a*. In general, the energy values based on DFT geometries, *i.e.* B3LYP, G3(MP2)B3 and G3B3, are in slightly better agreement with each other than with the energy values based on MP2 geometries, *i.e.* G2(MP2) and G3.

While the behavior of the different *ab initio* methods shows very good agreement for calculating preassociation energies, it shows more scattering for calculating reaction barriers, especially for the B3LYP/6-31+G(d) results. This is not unexpected, since DFT is well documented for underestimating reaction barriers (see Methods section). Comparing the Gaussian methods one finds that all methods coincide within 2 kcal mol^{-1} and the computationally most elaborate methods, namely G3 and G3B3, coincide within less than 0.5 kcal mol^{-1}. The coupled-cluster values are smaller throughout, possibly due to the different basis set. Transition states hardly converge for MP2 in some systems, independent of whether we used the 6-31G(d) or the aug-cc-pVDZ basis set. For further consideration we are therefore restricted to using methods based on B3LYP geometries. Thus, we use G3B3 values for the systems with $n = 1$ and $n = 2$ water molecules and G3(MP2)B3 values for the larger systems, since G3B3 would require an excessive amount of computer time and disk space for such systems. G3(MP2)B3 performs much better than B3LYP/6-31+G(d): it converges for all systems and it provides barriers that are within 1.5 kcal mol^{-1} compared to G3B3, so usage of G3(MP2)B3 seems justifiable. One can also expect, since there are no experimental reports on gas-phase reactions with more than two water molecules, that such processes will be of minor importance; thus the accuracy of the reported barriers are sufficient for our purposes.

Table 1 Upper table: electronic energies of preassociation [$N_2O_5 + nH_2O \leftrightarrows N_2O_5(H_2O)_n$] calculated at different levels of theory. Lower table: Gibbs standard state free energies for the preassociation at temperature 298.15 K, pressure 1.0 atm.[23]

	ΔE^{preass}/kcal mol^{-1}				
n	B3LYP	G2(MP2)	G3	G3(MP2)B3	G3B3
1*a*	−3.78	−3.36	−3.45	−4.45	−4.84
1*b*	−3.79[a]	−3.09	−3.34	−4.16	−4.59
2*a*	−11.76	−10.55	−11.28	−11.16	−12.20
2*b*,*c*	−13.03[a]	−11.75	−12.30	−12.44	−13.41
3*a*	−17.50	−16.85	—	−17.03	—
3*b*	−22.45	−20.05	—	−20.42	—
3*c*	−17.42	−16.81	—	−17.03	—
3*d*	−17.4[a]				
	ΔG^0_{preass}/kcal mol^{-1}				
n	B3LYP	G2(MP2)	G3	G3(MP2)B3	G3B3
1*a*	4.30	4.47	4.36	5.11	4.71
1*b*	4.62	3.55	3.81	4.44	4.09
2*a*	7.62	8.16	6.88	10.09	9.02
2*b*	7.52	5.52	4.96	7.23	6.35
3*a*	13.02	10.17	—	14.43	—
3*b*	9.45	7.18	—	11.56	—
3*c*	13.04	10.13	—	14.32	—

[a] See also Tao and co-workers.[23,24]

The coupled-cluster [CCSD(T)/aug-cc-pVDZ//MP2/aug-cc-pVDZ] calculations were examined by the $\mathcal{T}_1$ diagnostic, to find out whether the single determinant Hartree–Fock reference wave function describes the system satisfactorily.[39] The largest $\mathcal{T}_1$ value of 0.023 was obtained for the transition state of the $n = 1$ systems. $\mathcal{T}_1$ values of that size are clearly within the limit of 0.04 for CCSD(T).[39,59] Thus, the single determinant approach as used in coupled-cluster calculations is appropriate for the studied system.

Reaction barriers, but also preassociation energies, are crucial for predicting kinetic properties. Therefore, one has to be aware that within the accuracy of G3 and G3(MP2)B3 there is an error limit of a few kcal mol^{-1}. Assuming a total deviation of 3 kcal mol^{-1} we have to consider an error in terms of reaction rate constants of about two orders of magnitude at 300 K. To qualitatively compare theory with experiment this error limit is within an acceptable range. On the basis of the N_2O_5 molecule we compared geometrical parameters and vibrational frequencies with previous results of theoretical and experimental studies. These results are summed up in Tables 3 and 4. The B3LYP results for bond lengths are in better agreement with experiment than the MP2 results. Since energy calculations are very sensitive to small changes in the geometry, energy calculations based on B3LYP geometries are likely to be closer to the experimental value. This reaffirms our decision to use G3B3 and G3(MP2)B3 energies. The vibrational frequencies at the B3LYP/6-31+G(d) level of theory are in very good agreement with a previous theoretical study of Zhun *et al.*, who also also used B3LYP but the larger triple-zeta 6-311+G(2d) basis set. The B3LYP/6-31+G(d) frequencies are in reasonable agreement with the experimental ones, which was also found in a previous study.[23] (Tao and co-workers[23,24]

Table 2 Reaction barriers for the unimolecular transformation $[N_2O_5(H_2O)_n \leftrightarrow 2HNO_3(H_2O)_{n-1}]$ at different levels of theory. (Note: CCSD(T)/VDZ energies were calculated with the aug-cc-pVDZ basis set based on the geometries obtained at MP2/aug-cc-pVDZ; all values are without zero-point correction; values denoted with an asterisk (*) could not be obtained due to convergence problems for the transition state at the MP2 level)

	Reaction barrier/kcal mol^{-1}					
$n = 1$	B3LYP/6-31+G(d)	CCSD(T)/VDZ[c]	G2(MP2)	G3	G3(MP2)B3	G3B3
1*a*	13.91	18.76 (0.023)	20.14	20.88	22.26	21.07
1*b*	24.30[a]	27.79 (0.023)	28.97	29.81	30.77	29.81
2*a*	12.4	17.29 (0.022)	18.23	18.37	20.03	18.85
2*b*	17.49	*	*	*	25.05	23.41
2*c*	19.46[a]					
3*a*	9.90	—	*	*	14.23	—
3*b*	11.51[b]	—	*	*	19.01	—
3*c*	13.50	—	*	*	19.23	—
3*d*	10.4[a]					

[a] See also Tao and co-workers.[23,24] [b] See McNamara and Hillier.[25] [c] $\mathscr{T}_1$ values at the transition state in parenthesis.

reported also that the B3LYP/6-31+G(d) values converged with respect to basis set for geometries and energies since the results obtained with the 6-31+G(d) basis set are in excellent agreement with the 6-311++G(d,p) basis set.) The HF/6-31G(d) frequencies (as used in the Gaussian approaches), however, are worse than the DFT results. Yet, scaling of the Hartree–Fock values by 0.89,[32,33] as performed in the G2 and G3 approaches, make the Hartree–Fock harmonic frequencies almost as good as the B3LYP/6-31+G(d) frequencies. Due to the good performance of B3LYP/6-31+G(d) we used the harmonic frequencies at this level of theory along the minimum energy path.

3.2 Stationary points

3.2.1 $N_2O_5 + 1H_2O$. We characterized two different reaction channels or mechanisms of the hydrolysis of N_2O_5 with one molecule of water and consequently two transition states (see Figs. 1 and 2). The different mechanisms are termed 1*a* and 1*b* and the analogous nomenclature will be used throughout the rest of this study. Structurally, the reaction complex (RC) in 1*a* differs from the RC in 1*b* since in 1*a* the water molecule is almost perpendicular to the bridging oxygen atom of N_2O_5, whereas in 1*b* the water molecule is nearly perpendicular to one of the NO_3 groups. Mechanism 1*b* is equivalent to the one reported by Hanway and Tao,[23] whereas 1*a* has not been described in the literature yet. The energies of association for both RC 1*a* and RC 1*b* differ by less than 0.3 kcal mol^{-1} (see Table 1, G3B3 values). The standard state free energy of association at 298.15 K (ΔG^0_{preass}) is endergonic for both complexes, and 1*b* is energetically lower by 0.6 kcal mol^{-1}, making it the slightly more favorable complex at standard conditions even though the pure electronic energy favors RC 1*a* (see Table 1). The mechanism and geometrical details of reaction channel 1*b* have already been characterized in detail: thus we refer to the studies of Tao and co-workers[23,24] and highlight the new mechanism in comparison to the old one.

In both mechanisms the reaction proceeds *via* a nucleophilic attack by the water molecule on N_2O_5 (see Fig. 1). The transition state (TS) structures are similar, yet, in 1*a*, one nitrate group rotates approximately 60° more along one N–O bond than in 1*b* (see Fig. 2). Due to this rotation the water molecule forms a complex with the NO_2 acceptor group which, in turn, will react with the OH moiety of water to form the first HNO_3 molecule. At the same time the remaining water H forms a linear hydrogen bond with the NO_3 group that will form the second HNO_3. The corresponding hydrogen bond in 1*b* is deformed from linearity by 30°. Thus, the TS in 1*a* is more stabilized by this hydrogen bond. This, in turn, lowers the reaction barrier remarkably from 29.8 kcal mol^{-1} (1*b*) to 21.1 kcal mol^{-1} (1*a*). Even though formation of the RC 1*b* is favored by 0.3 kcal mol^{-1} compared to RC 1*a* the higher barrier of 8.7 kcal mol^{-1} makes reaction channel 1*a* the more likely one.

3.2.2 $N_2O_5 + 2H_2O$. Similarly, we found two different reaction channels for the hydrolysis of N_2O_5 with $n = 2$ water molecules named 2*a* and 2*b* (see Fig. 1). Unfortunately, we were not able to characterize the same reaction mechanism as was described by Hanway and Tao[23] (2*c*) since the transition state did not converge. Yet, interestingly the RC 2*b* described in this study is identical to RC 2*c* of Hanway and Tao, even though the corresponding transition state 2*b* differs from 2*c*. Apparently, this reaction complex is connected with two different transition states and thus two different minimum energy paths. Hanway and Tao described mechanism 2*c* at the B3LYP/6-31+G(d) level, which is identical to one of our levels and found a barrier of 19.5 kcal mol^{-1}. At this level, both of the new mechanisms have much lower barriers and both are saddle points of first order with one imaginary frequency each [217.7i and 496.6i, B3LYP/6-31+G(d)]. Unfortunately it is not possible to compare the barriers at higher levels of theory but at least the energy of pre-association is known at the different

Table 3 Geometric parameters for N_2O_5 in comparison with previous theoretical and experimental studies

	B3LYP			MP2		
	6-31+G(d)[a b]	6-311++G(d,p)[a]	6-31G(d)[a]	6-31G(d)[b]	aug-cc-pVDZ[b]	Expt.[c]
r (N–O)	1.508	1.512	1.505	1.528	1.539	1.492(4)
r (N=O)	1.196	1.189	1.196	1.207	1.203	1.183(2)
∠ r O=N=O	133.3	133.4	133.2	133.8	134.0	133.2(6)
∠ N–O–N	114.7	115.0	114.4	111.9	111.5	111.8(2)
∠ O–N=O_1	116.6	116.4	116.7	116.2	116.0	–

[a] Values taken from Hanway and Tao.[23] [b] Values from this study. [c] Values from McClelland *et al.*[64]

Table 4 Vibrational frequencies of N_2O_5 in comparison with experiment and previous experimental studies

		B3LYP		
Assignment[a]	Expt.	6-31+G(d)	6-311+G(2d)[b]	HF/6-31G(d)
ν_1, ν_{11}	1728	1830	1792	2011
ν_1	1728	1787	1792	1958
ν_2	1338	1398	1382	1619
ν_{12}	1247	1303	1286	1501
ν_{13}	860	877	886	1068
		799	811	994
ν_3, ν_{14}	743	741	753	964
		724	740	863
ν_4	614	670	683	837
ν_9	577	562	568	782
		379	381	575
ν_5	353	347	345	506
		217	219	277
ν_6	85	63	62	89
		51	48	9

[a] Assignment of vibrations and experimental values according to Hisatsune *et al.*[65] [b] Values at B3LYP/6-311+G(2d) level are taken from Zhun *et al.*[66]

levels. The standard state free energy for pre-association favors 2*b* and 2*c* by 2.7 kcal mol^{-1} over 2*a* and also the energy of pre-association is in favor of 2*b* and 2*c*.

From the mechanistic point of view, 2*a* and 2*c* are reactions of N_2O_5 with two molecules of water, one of which is the reaction partner and the other a spectator that catalyzes the reaction through its hydrogen bonds (see also Fig. 2). In mechanism 2*b* both water molecules participate actively in the reaction where one molecule transfers one of its protons to the second water molecule and the remaining one forms HNO_3 with the NO_{2-} subgroup. The protonated water molecule in turn transfers one of its own protons to the nitrate group and forms the second HNO_3 entity.

3.2.3 $N_2O_5 + 3H_2O$. Again, two new mechanisms could be identified. Tao and co-workers[24] have characterized a mechanism (which we will refer of 3*d*) which we were again not able to characterize due to convergence problems at the transition state. A second mechanism for N_2O_5 hydrolysis with three water molecules has been reported by McNamara and Hillier[25] which we also characterized and which we term 3*b* (see Fig. 1). The RC for this mechanism turned out to be the lowest lying minimum structure of all four reaction complexes. However, this reaction mechanism is not the one with the lowest reaction barrier, which is the one for mechanism 3*a*. Unlike our barrier for mechanism 3*b*, McNamara and Hillier report a value of 13.4 kcal mol^{-1} at their highest level of theory [MP2/6-311++G(3df,3dp)//B3LYP/6-311++G(d,p)] which is 7.5 kcal mol^{-1} lower than our best guess. It is difficult to judge which value is "better"; however, for the purpose of comparison and since there were several difficulties with convergence at the MP2 level, we use our G3(MP2)B3 results in the rest of this study.

The reaction barrier of the mechanism reported by Snyder *et al.*[24] is quite low at the B3LYP/6-31+G(d) level (10.4 kcal mol^{-1}) and it is probable that at higher levels of theory it would be higher. Mechanistically, in none of the reaction channels do all three water molecules participate actively in the course of the reaction. In mechanisms 3*a* and 3*b* only one water molecule acts as a spectator whereas in 3*c* two water molecules are passive during the reaction. 3*c* is an extension of 2*b* and the effect of the additional water molecule lowers the reaction barrier by almost 6 kcal mol^{-1}. 3*a* is an extension of mechanism 1*a* and the barrier is lower by 8 kcal mol^{-1}.

3.3 Reaction rate constants

Previous theoretical studies on N_2O_5 hydrolysis have described reaction barriers but no reaction rate constants. Additionally, these studies did not include reactions that start from a slightly higher lying local minimum but have lower barriers. To accurately predict reaction rates the reaction barrier is not sufficient even if we are only interested in a qualitative and not a

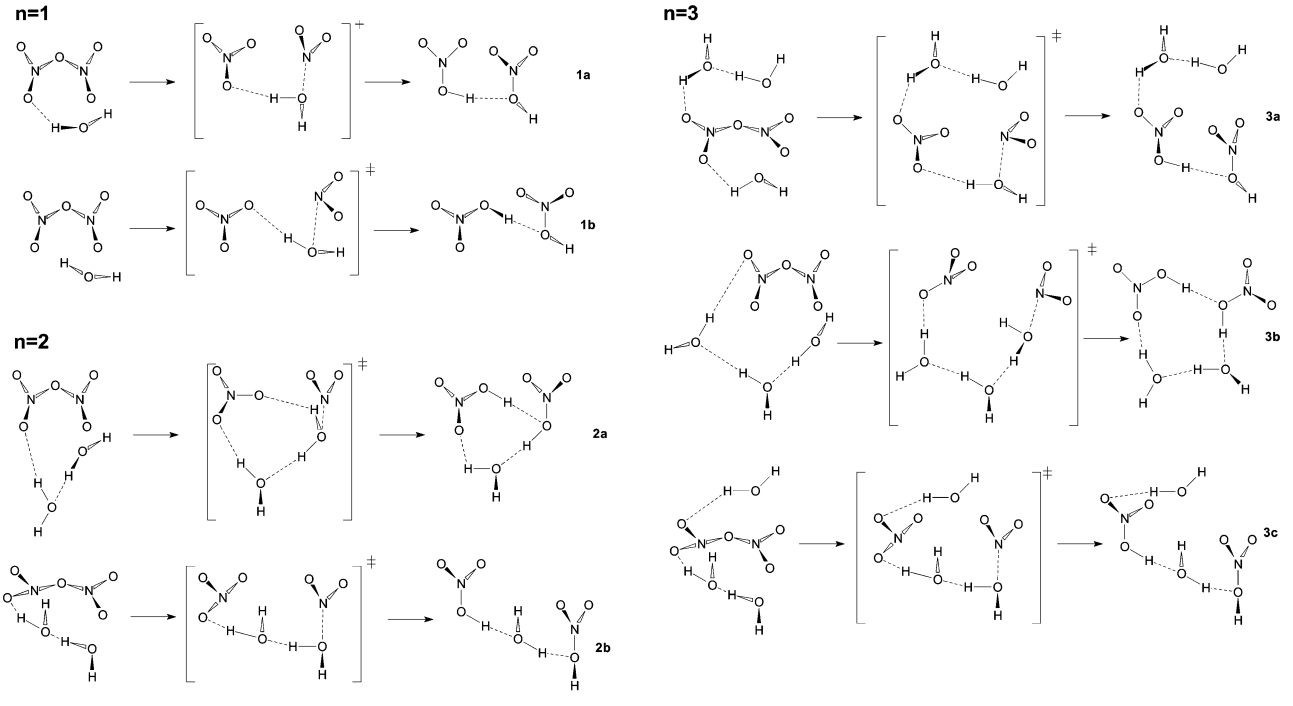

Fig. 1 Qualitative representation of the stationary points of the hydrolysis reaction of N_2O_5 with one, two, and three water molecules. Mechanisms 1*a*, 2*a*, 2*b*, 3*a* and 3*c* are new (this study), whereas 1*b* is the same as in Hanway and Tao[23] and 3*b* is the same as in McNamara and Hillier.[25] (Left: reactants; middle: transition states; right: products.)

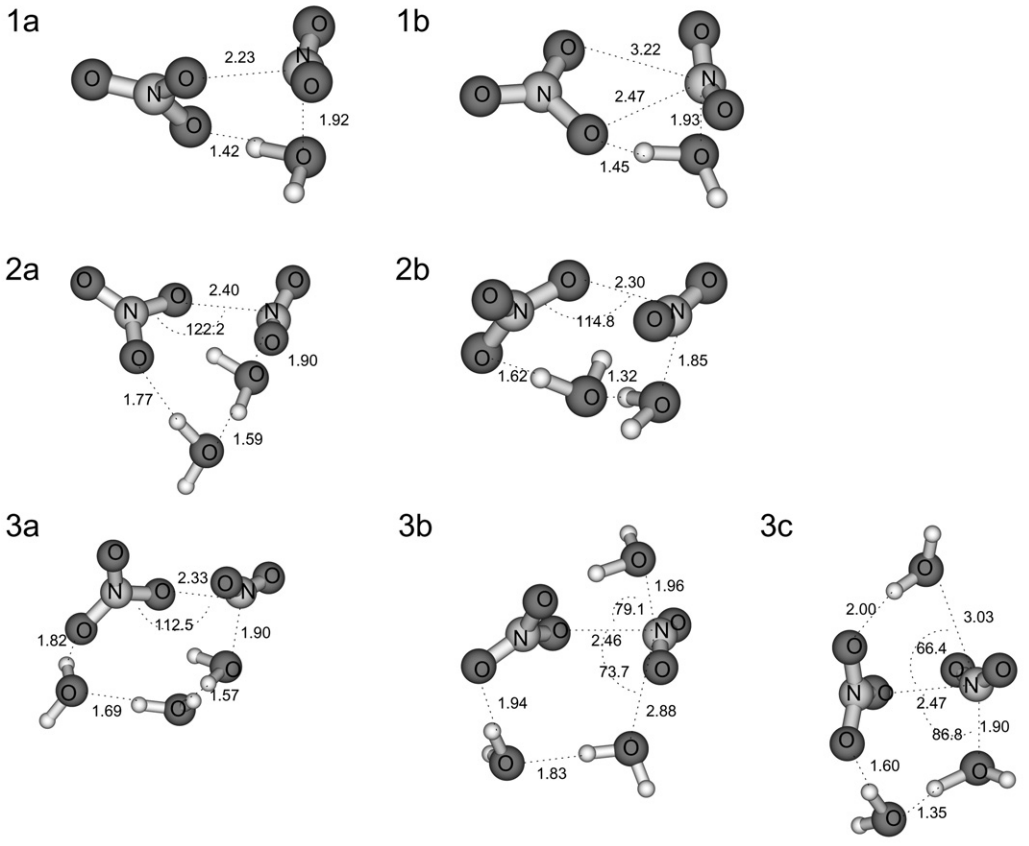

Fig. 2 Structure of the transition states of the different hydrolysis mechanisms. In mechanisms 2*a*, 3*a* and 3*b* only one water molecule is actively involved in the reaction whereas the remaining water molecule(s) are spectators. In 2*b* and 3*c* two water molecules are actively involved in the reaction where the second water molecule donates one of its own protons after is protonated by the first water molecule. The third water molecule in 3*c* is again just a spectator molecule.

quantitative picture. An accurate calculation of rate constants for reactions involving hydrogen atom transfer requires a quantum mechanical treatment of the motion along the reaction coordinate. Thus, information on the potential energy surface beyond the barrier height is required. It turned out that tunneling can increase the reaction rate by many orders of magnitude[60–63] if there is at least one proton transfer involved. Therefore we determined tunneling contributions on the reaction rates for the described reactions.

Fig. 3 shows the unimolecular rate constants of the N_2O_5 hydrolysis supported by $n = 1$ to $n = 3$ water molecules as a function of temperature. The reaction rate constant increases with an increasing number of water molecules due to the lowering of the reaction barrier. However, the unimolecular rate constant considers the reaction rate constant only after formation of a reaction (or preassociation) complex. Additionally, identification and an appropriate treatment of internal hindered rotations has a strong influence on the overall reaction rate constant. To compare theoretical and experimental values, one has to consider the whole reaction, including formation of the reaction complex. In Fig. 4 the second, third, and fourth order reaction rate constants for the N_2O_5 hydrolysis according to the mechanisms

$$N_2O_5 + H_2O \leftrightarrows 2HNO_3 \quad (6)$$

$$N_2O_5 + 2H_2O \leftrightarrows 2HNO_3 + H_2O \quad (7)$$

$$N_2O_5 + 3H_2O \leftrightarrows 2HNO_3 + 2H_2O \quad (8)$$

are shown which include the preassociation equilibrium for the reaction complex formation; the results are compared to the experimental values.

The results with one water molecule show that the rate constant determined with the new mechanism (1*a*) is in much better agreement with experiment than with the old mechanism (1*b*) (see Table 5).[23,24] Compared to experiment, the reaction rate constant at 293 K of the old mechanism is almost ten orders of magnitude smaller than the currently best experimental value. For the new mechanism the rate constant is only two orders of magnitude smaller[22] (see Table 5). Under standard conditions mechanism 1*a* is the predominant reaction mechanism. Without treating hindered rotations adequately, the rate constants are 5.4×10^{-28} (298 K) for 1*a* and 9.9×10^{-34} (298 K) for 1*b*. The large difference of three orders of magnitude for mechanism 1*a* pinpoints the necessity to take hindered rotations into consideration.

With two water molecules it is more difficult to judge which mechanism will be the predominant one. Compared to experiment, reaction channel 2*a* and 2*b* both are about seven orders of magnitude smaller. Since we were not able to determine the exact rate constant for 2*c*, we can only estimate the reaction rate for this mechanism in comparison to the others. Assuming that a high level barrier would be 6.1 kcal mol^{-1} higher than the B3LYP/6-31+G(d) value, the proposed mechanism would have an estimated barrier of 25.6 kcal mol^{-1}. The value of 6.1 kcal mol^{-1} is the mean deviation of the barrier determined at the B3LYP/6-31+G(d) level compared with the best guess. With this value we can do a conservative TST guess which would yield a rate constant of 5.9×10^{-51} cm^6 $molecule^{-2}$ s^{-1} at 298 K. This value is more than three orders of magnitude slower than the other two mechanisms (see Table 5).

We have also investigated mechanisms with three water molecules even though it is quite unlikely that four molecules meet randomly to form a reaction complex. Mechanism 3*a*

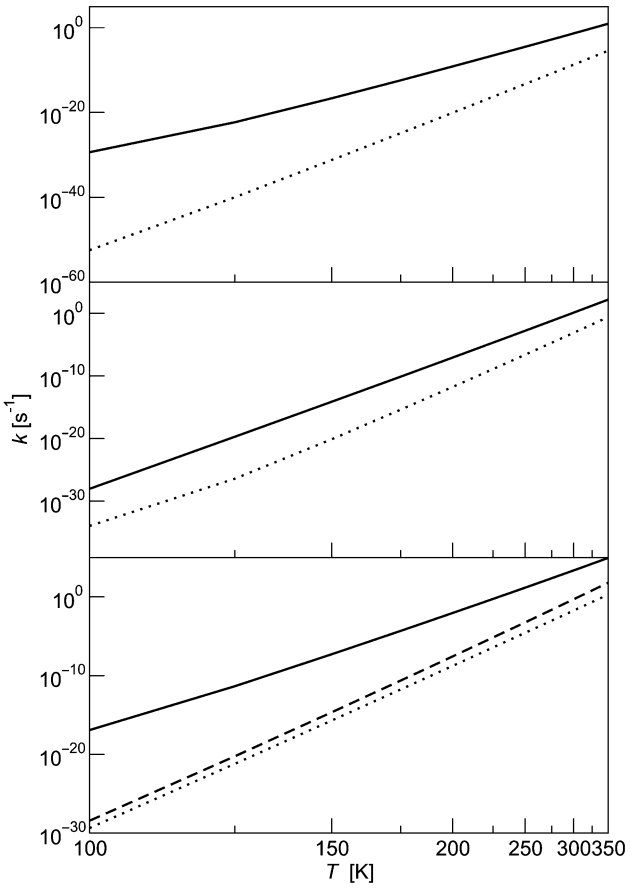

Fig. 3 Unimolecular reaction rates of the reaction $N_2O_5(H_2O)_n \leftrightarrows 2HNO_3(H_2O)_{n-1}$ as obtained by VTST/μOMT. Mechanism *a* full, *b* dotted and *c* broken line. Mechanism *a* is fastest for all systems. The unimolecular reaction rate constants increase with increasing number of water molecules but this effect is not very great.

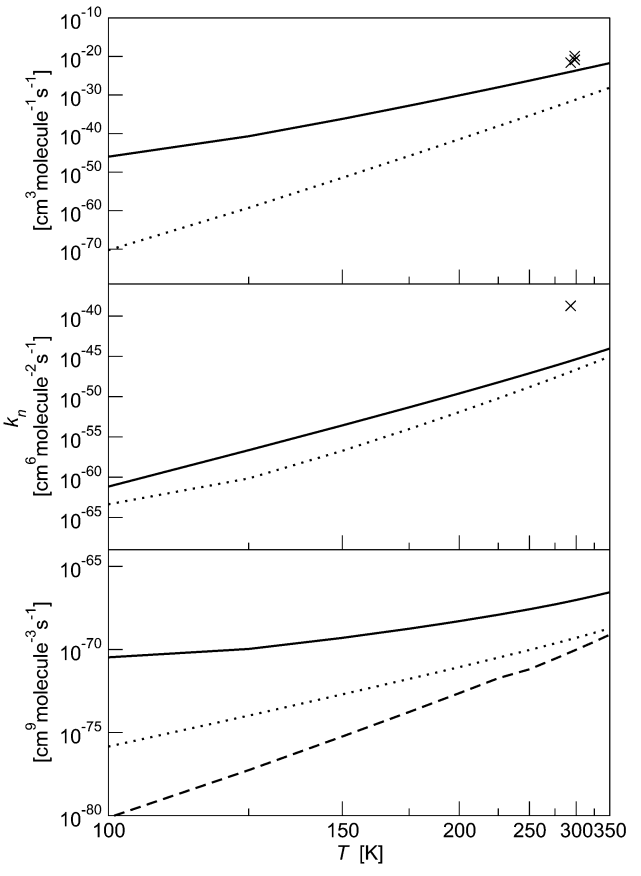

Fig. 4 Comparison of the bi-, tri-, and tetramolecular reaction rate constants of N_2O_5 hydrolysis. The values denoted with an $\times$ are the experimental values as summed up in Table 5. The new mechanism with one water molecule is in much better agreement with the experimental value than with the old mechanism. The mechanisms with two water molecules are almost equally important. For three water molecules, again mechanism *a* is the fastest one, as for the unimolecular rate constants, whereas for mechanism 3*c* the tetramolecular rate constant becomes slower than 3*b*, in contrast to the unimolecular rate constants (*a* full line, *b* dotted line, *c* broken line).

would be the most important one, being about two orders of magnitude faster than the other two mechanisms. 3*d* might be equally important: however, with the limited data this is difficult to judge.

3.4 Kinetic isotope effects

One way to find out which reaction mechanism predominates could be to determine the kinetic isotope effects (KIE) of this reaction and to compare experimental and theoretical values. Unfortunately, there have been no reports on experimental KIEs.

Table 6 lists the theoretical KIEs for all investigated reaction mechanisms at standard conditions. The values for the KIE are all relatively small, so we took a more detailed look at the the contribution of quantum mechanical tunneling on the reaction rate constants. At standard conditions the tunneling contributions are small—all below a factor of 1.6 (see Table 7). At lower temperatures, however, tunneling is much more important and at 190 K, for instance, the tunneling correction becomes 3.2 for reaction 1*b*, which indicates that the rate of reaction is enhanced by 220% due to tunneling. The most important form of tunneling is small-curvature tunneling throughout all mechanisms, which seems not surprising on inspection of Fig. 5. The minimum energy paths of all reactions are relatively broad, which is typical for reactions where small curvature tunneling is predominant.

4 Conclusion

The reaction of N_2O_5 with water has been investigated theoretically by *ab initio* methods and variational transition state theory. New reaction mechanisms for the reaction with $n = 1$, $n = 2$ and $n = 3$ water molecules are shown. Especially the second order rate constant (first order with respect to $[H_2O]$ and first order with respect to $[N_2O_5]$) deduced from the new mechanism is in better agreement with the currently best experimental upper limit rate constant than the rate constant deduced by the old mechanism. The difference between theory and experiment is not disconcertingly large. Wahner *et al.*[22] report that there is only a small error potential left in

Table 5 Comparison between experiment and theory of the reaction rate constants for the reaction of $N_2O_5 + nH_2O \leftrightarrows 2HNO_3 + (n-1)$-$H_2O$. The rate constants are first order with respect to N_2O_5 and nth order with respect to H_2O. The two "theory" values for $n = 2$ correspond to mechanisms 2*a* and 2*b*. (Pre-association complex obtained at G3B3 level of theory, unimolecular reaction rates obtained at a G3B3///B3LYP/6-31+G(d) hypersurface.)

	$n = 1$ / cm^3 molecule^{-1} s^{-1}	$n = 2$ / cm^6 molecule^{-2} s^{-1}
Morris and Niki, 1973[17]	1.3×10^{-20} (298 K)	—
Tuazon *et al.*, 1983[18]	1.3×10^{-21} (298 K)	—
Atkinson *et al.*, 1986[19]	$\leq 1.5 \times 10^{-21}$ (298 K)	—
Mentel *et al.*, 1996[21]	2.6×10^{-22} (293 K)	1.9×10^{-39} (293 K)
Wahner *et al.*, 1998[22]	2.5×10^{-22} (293 K)	1.8×10^{-39} (293 K)
Theory (this work)	5.2×10^{-25} (298 K)	4.3×10^{-46} (298 K)
		2.2×10^{-47} (298 K)

Table 6 Kinetic isotope effects for the different reaction mechanisms at 298.15 K

Mechanism	1*a*	1*b*	2*a*	2*b*	3*a*	3*b*	3*c*
KIE	1.55	1.09	1.11	1.44	1.31	1.87	1.29

Table 7 Transmission coefficients κ for the different reaction mechanisms at 190 and 298 K. Small curvature tunneling is the predominant form of tunneling at for all mechanisms

T/K	1*a*	1*b*	
190.00	1.982	3.248	
298.15	1.296	1.538	
	2*a*	2*b*	
190.00	1.133	2.085	
298.15	1.052	1.324	
	3*a*	3*b*	3*c*
190.00	1.601	1.382	1.494
298.15	1.194	1.135	1.163

the experimental approach. However, there are uncertainties of 2–3 kcal mol^{-1} in the theoretical approach and thus there is an error potential of two orders of magnitude in terms of reaction rate constants. Presently it is not possible to clarify whether the proposed mechanism is also the predominant one in experimentation. From the experimental point of view KIEs or a broader investigated temperature range might give first evidence whether the proposed reaction channels are the most important ones and if they compare well with experiment. From the mechanistic point of view, in reaction channels with more than one water molecule, water was found either to participate actively mediating proton transfer or to be just a spectator that stabilizes the transition state. Energetically it was found that there are reaction mechanisms that are more likely than others, even though the reaction complex is in a "higher" local minimum that is still populated under standard conditions. Several low frequency vibrations were identified as hindered rotations. Treating these hindered rotations with the approximation developed by Truhlar[42,44] had a strong effect on the rate constants, lowering the discrepancy between theory and experiment from six to only two orders of magnitude. It was also shown that B3LYP/6-31+G(d) performs very well in predicting vibrational frequencies and geometries but it fails to predict reaction barriers accurately. Perturbation theory (MP2) proved to be problematic with respect to convergence in transition state geometry optimization.

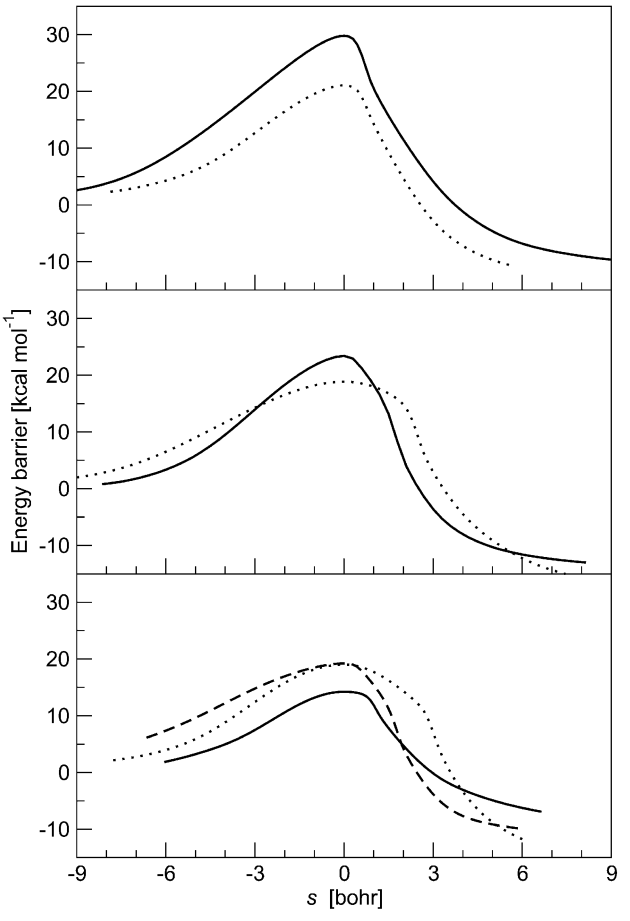

Fig. 5 Minimum energy paths for the reaction of N_2O_5 with *n* water molecules. The abscissa marks the progress of the reaction with $s = 0$ being the transition state, $s < 0$ being reactant-like and $s > 0$ product-like species. (The path was calculated at B3LYP/6-31+G(d) level of theory and interpolated to G3B3 ($n = 1,2$) or G3(MP2)B3 energies.)

Acknowledgements

We are grateful to one of the referees for recommending treating hindered rotations appropriately. This study was supported by the Austrian Science Fund (project number P14357-TPH).

References

1 J. M. Rodriguez, M. K. W. Ko and N. D. Sze, *Nature*, 1991, **352**, 134–137.
2 P. O. Wennberg, R. C. Cohen, R. M. Stimpfle, J. P. Koplow, J. G. Anderson, R. J. Salawitch, D. W. Fahey, E. L. Woodbridge, E. R. Keim, R. S. Gao, C. R. Webster, R. D. May, D. W. Toohey, L. M. Avallone, M. H. Proffitt, M. Loewenstein, J. R. Podolske, K. R. Chan and S. C. Wofsy, *Science*, 1994, **266**, 398–404.
3 P. J. Crutzen, J.-U. Grooß, C. Brühl, R. Müller and J. M. Russell III, *Science*, 1995, **268**, 705–708.
4 D. W. Fahey and A. R. Ravishankara, *Science*, 1999, **285**, 208–211.
5 P. J. Crutzen and F. Arnold, *Nature*, 1986, **324**, 651–655.
6 C. R. Webster, R. D. May, R. Toumi and J. A. Pyle, *J. Geophys. Res.*, 1990, **95**, 13 851–13 866.
7 J. Hahn, K. Luther and J. Troe, *Phys. Chem. Chem. Phys.*, 2000, **2**, 5098–5104.
8 C. D. Nevison, S. Solomon and J. M. Russell III, *J. Geophys. Res.*, 1996, **101**, 6741–6748.
9 J. B. Kumer, S. R. Kawa, A. E. Roche, J. L. Mergenthaler, S. E. Smith, F. W. Taylor, P. S. Connell and A. R. Douglass, *J. Geophys. Res.*, 1997, **102**, 3575–3582.
10 P. J. Crutzen, *Q. J. R. Meteorol. Soc.*, 1970, **96**, 320–327.
11 H. S. Johnston, *Science*, 1971, **173**, 517–522.
12 P. J. Crutzen and C. Brühl, *J. Phys. Chem. A*, 2001, **105**, 1579–1582.
13 S. Solomon, *Rev. Geophys.*, 1999, **37**, 275–316.
14 M. B. McElroy, R. J. Salawitch, S. C. Wofsy and J. A. Logan, *Nature*, 1986, **321**, 759–762.
15 M. B. McElroy, J. Salawitch and K. Minschwaner, *Planet. Space Sci.*, 1992, **40**, 373–401.
16 R. Atkinson, D. L. Baulch, R. A. Cox, R. F. Hampson, J. A. Kerr, M. J. Rossi and J. Troe, *J. Phys. Chem. Ref. Data*, 1997, **26**, 521–1011.
17 J. E. D. Morris and H. Niki, *J. Phys. Chem.*, 1973, **77**, 1929–1932.
18 E. C. Tuazon, R. Atkinson, C. N. Plum, A. M. Winer, J. James and N. Pitts, *Geophys. Res. Lett.*, 1983, **10**, 953–956.
19 R. Atkinson, E. C. Tuazon, H. MacLeod, S. M. Aschmann and A. M. Winer, *Geophys. Res. Lett.*, 1986, **13**, 117–120.
20 J. Hjorth, G. Ottobrini, F. Cappellani and G. Restelli, *J. Phys. Chem.*, 1987, **91**, 1565–1568.
21 T. F. Mentel, D. Bleilebens and A. Wahner, *Atmos. Environ.*, 1996, **30**, 4007–4020.
22 A. Wahner, T. F. Mentel and M. Sohn, *Geophys. Res. Lett.*, 1998, **25**, 2169–2172.

23 D. Hanway and F.-M. Tao, *Chem. Phys. Lett.*, 1998, **285**, 459–466.
24 J. A. Snyder, D. Hanway, J. Mendez, A. J. Jamka and F.-M. Tao, *J. Phys. Chem. A*, 1999, **103**, 9355–9358.
25 J. P. McNamara and I. H. Hillier, *J. Phys. Chem. A*, 2000, **104**, 5307–5319.
26 P. J. Stephens, F. J. Devlin, C. F. Chabalowski and M. J. Frisch, *J. Phys. Chem.*, 1994, **45**, 11 623–11 627.
27 C. Peng, P. Y. Ayala and H. B. Schlegel, *J. Comput. Chem.*, 1996, **17**, 49–56.
28 J. L. Durant, *Chem. Phys. Lett.*, 1996, **256**, 598–602.
29 B. S. Jursic, *J. Mol. Struct. (Theochem)*, 1997, **417**, 89–94.
30 B. J. Lynch, P. L. Fast, M. Harris and D. G. Truhlar, *J. Phys. Chem. A*, 2000, **104**, 4811–4815.
31 L. A. Curtiss, K. Raghavachari, G. W. Trucks and J. A. Pople, *J. Chem. Phys.*, 1991, **94**, 7221–7230.
32 L. A. Curtiss, K. Raghavachari and J. A. Pople, *J. Chem. Phys.*, 1993, **98**, 1293–1298.
33 L. A. Curtiss, K. Raghavachari, P. C. Redfern and J. A. Pople, *J. Chem. Phys.*, 1998, **109**, 7764–7776.
34 A. G. Baboul, L. A. Curtiss, P. C. Redfern and K. Raghavachari, *J. Chem. Phys.*, 1999, **110**, 7650–7657.
35 L. A. Curtiss, P. C. Redfern, K. Raghavachari, V. Rassolov and J. A. Pople, *J. Chem. Phys.*, 1999, **110**, 4703–4709.
36 K. Raghavachari, G. W. Trucks, J. A. Pople and M. Head-Gordon, *Chem. Phys. Lett.*, 1989, **157**, 479–483.
37 C. Møller and M. S. Plesset, *Phys. Rev.*, 1934, **46**, 618–622.
38 T. H. Dunning, Jr., *J. Chem. Phys.*, 1989, **90**, 1007–1023.
39 T. J. Lee and P. R. Taylor, *Int. J. Quantum Chem. Quantum Chem. Symp.*, 1989, **23**, 199–207.
40 Y.-Y. Chuang and D. G. Truhlar, *J. Chem. Phys.*, 2000, **112**, 1221–1228.
41 P. Y. Ayala and H. B. Schlegel, *J. Chem. Phys.*, 1998, **108**, 2314–2325.
42 D. G. Truhlar, *J. Comput. Chem.*, 1991, **12**, 266–270.
43 M. Page and J. W. McIver, Jr., *J. Chem. Phys.*, 1988, **88**, 922–935.
44 Y.-Y. Chuang and D. G. Truhlar, *J. Phys. Chem. A*, 1997, **101**, 3808–3814.
45 H. Eyring, *J. Chem. Phys.*, 1935, **3**, 107–115.
46 J. C. Corchado, Y.-Y. Chuang, P. L. Fast, J. Villá, W.-P. Hu, Y.-P. Liu, G. C. Lynch, K. A. Nguyen, C. F. Jackels, V. S. Melissas, B. J. Lynch, I. Rossi, E. L. Coitiño, A. Fernandez-Ramos, J. Pu, T. V. Albu, R. Steckler, B. C. Garrett, A. D. Isaacson and D. G. Truhlar, Polyrate9.0, University of Minnesota, Minneapolis, 2002.
47 J. C. Corchado, Y.-Y. Chuang, E. L. Coitiño, D. G. Truhlar, Gaussrate9.0, University of Minnesota, Minneapolis, 2002.
48 D. G. Truhlar and B. C. Garrett, *Ann. Rev. Phys. Chem.*, 1984, **35**, 159–189.
49 D. G. Truhlar, A. D. Isaacson and B. C. Garrett, in *Theory of Chemical Reaction Dynamics*, ed. M. Baer, CRC Press, Boca Raton, FL, 1985, ch. Generalized Transition State Theory, pp. 65–137.
50 M. M. Kreevoy and D. G. Truhlar, in *Investigation of Rates and Mechanisms of Reactions*, ed. C. F. Bernasconi, John Wiley & Sons, Inc., New York, 1986, ch. Transition State Theory, pp. 13–95.
51 S. C. Tucker, D. G. Truhlar, in *New Theoretical Concepts for Understanding Organic Reactions*, NATO ASI Series C 267, ed. J. Bertrán and I. G. Csizmadia, Kluwer, Dordrecht, The Netherlands, 1989, ch. Dynamical Formulation of Transition State Theory: Variational Transition States and Semiclassical Tunneling, pp. 291–346.
52 D. G. Truhlar, B. C. Garrett and S. J. Klippenstein, *J. Phys. Chem.*, 1996, **100**, 12 771–12 800.
53 R. A. Marcus and M. E. Coltrin, *J. Chem. Phys.*, 1977, **67**, 2609.
54 R. T. Skodje, D. G. Truhlar and B. C. Garrett, *J. Phys. Chem.*, 1981, **85**, 3019–3023.
55 K. K. Baldridge, M. S. Gordon, R. Steckler and D. G. Truhlar, *J. Phys. Chem.*, 1989, **93**, 5107–5119.
56 A. Fernández-Ramos and D. G. Truhlar, *J. Chem. Phys.*, 2001, **114**, 1491–1496.
57 T. Loerting and K. R. Liedl, *Proc. Natl. Acad. Sci.*, 2000, **97**, 8874–8878.
58 M. J. Frisch, G. W. Trucks, H. B. Schlegel, G. E. Scuseria, M. A. Robb, J. R. Cheeseman, V. G. Zakrzewski, J. A. Montgomery, R. E. Stratmann, J. C. Burant, S. Dapprich, J. M. Millam, A. D. Daniels, K. N. Kudin, M. C. Strain, O. Farkas, J. Tomasi, V. Barone, M. Cossi, R. Cammi, B. Mennucci, C. Pomelli, C. Adamo, S. Clifford, J. Ochterski, G. A. Petersson, P. Y. Ayala, Q. Cui, K. Morokuma, D. K. Malick, A. D. Rabuck, K. Raghavachari, J. B. Foresman, J. Cioslowski, J. V. Ortiz, B. B. Stefanov, G. Liu, A. Liashenko, P. Piskorz, I. Komaromi, R. Gomperts, R. L. Martin, D. J. Fox, T. Keith, M. A. Al-Laham, C. Y. Peng, A. Nanayakkara, M. Challacombe, P. M. W. Gill, B. Johnson, W. Chen, M. W. Wong, J. L. Andres, C. Gonzalez, M. Head-Gordon, E. S. Replogle and J. A. Pople, *Gaussian 98, Revision A.9*, Gaussian, Inc., Pittsburgh, PA, 1998.
59 P. R. Taylor, in *European Summerschool in Quantum Chemistry*, ed. B. O. Roos and P.-O. Widmark, Lund University, Lund, Sweden, 2000, ch. Coupled-Cluster Methods in Quantum Chemistry, pp. 361–430.
60 T. Loerting, K. R. Liedl and B. M. Rode, *J. Am. Chem. Soc.*, 1998, **120**, 404–412.
61 T. Loerting, K. R. Liedl and B. M. Rode, *J. Chem. Phys.*, 1998, **109**, 2672–2679.
62 T. Loerting and K. R. Liedl, *Chem. Eur. J.*, 2001, **7**, 1662–1669.
63 C. S. Tautermann, A. F. Voegele, T. Loerting, I. Kohl, A. Hallbrucker, E. Mayer and K. R. Liedl, *Chem. Eur. J.*, 2002, **8**, 66–73.
64 B. W. McClelland, L. Hedberg, K. Hedberg and K. Hagen, *J. Am. Chem. Soc.*, 1983, **105**, 3789–3793.
65 I. C. Hisatsune, J. P. Devlin and Y. Wada, *Spectrochim. Acta*, 1962, **18**, 1641–1653.
66 I. Zhun, X. Zhou and R. Liu, *J. Chem. Phys.*, 1996, **105**, 11 366–11 367.